

Tip localization of an atomic force microscope in transmission microscopy with nanoscale precision

Fabian Baumann,¹ Stephan F. Heucke,² Diana A. Pippig,^{1,a)} and Hermann E. Gaub¹

¹Center for Nanoscience and Department of Physics, University of Munich, Amalienstraße 54, 80799 Munich, Germany

²Center for Integrated Protein Science Munich (CIPSM), University of Munich, Butenandtstraße 5-13, 81377 Munich, Germany

(Received 11 January 2015; accepted 5 March 2015; published online 20 March 2015)

Since the atomic force microscope (AFM) has evolved into a general purpose platform for mechanical experiments at the nanoscale, the need for a simple and generally applicable localization of the AFM cantilever in the reference frame of an optical microscope has grown. Molecular manipulations like in single molecule cut and paste or force spectroscopy as well as tip mediated nanolithography are prominent examples for the broad variety of applications implemented to date. In contrast to the different kinds of superresolution microscopy where fluorescence is used to localize the emitter, we, here, employ the absorbance of the tip to localize its position in transmission microscopy. We show that in a low aperture illumination, the tip causes a significant reduction of the intensity in the image plane of the microscope objective when it is closer than a few hundred nm. By independently varying the z-position of the sample slide, we could verify that this diffraction limited image of the tip is not caused by a near field effect but is rather caused by the absorbance of the transmitted light in the low apex needle-like tip. We localized the centroid position of this tip image with a precision of better than 6 nm and used it in a feedback loop to position the tip into nano-apertures of 110 nm radius. Single-molecule force spectroscopy traces on the unfolding of individual green fluorescent proteins within the nano-apertures showed that their center positions were repeatedly approached with very high fidelity leaving the specific handle chemistry on the tip's surface unimpaired. © 2015 AIP Publishing LLC. [<http://dx.doi.org/10.1063/1.4915145>]

I. INTRODUCTION

The atomic force microscope (AFM) plays an increasingly important role in numerous research fields ranging from nano-sciences where they initially were developed for material research and life sciences.^{1,2} Originally utilized for topographic surface imaging, this microscope technique evolved as an indispensable tool for spectroscopic analysis of mechanical, electric, or even magnetic surface properties.^{3,4} Besides, its capability to employ forces in the realm of inter- or intramolecular bonds opened up an entire research field of biophysical applications: from single-molecule force spectroscopy to the controlled manipulation and rearrangement of bio-molecular components on the single-molecule level.⁵⁻⁸

Since the first controlled nano-manipulation of individual xenon atoms by a scanning tunneling microscope,^{9,10} the idea of an AFM performing as a robotic arm with nanometer accuracy became increasingly popular particularly for the characterization and assembly of nano-objects with utmost precision.^{11,12} While the force-resolution has been pushed to sub-pN accuracy¹³ and the spatial position may be actively controlled with atomic precision,¹⁴ AFM operations in a lab-coordinate system (i.e., the coordinate system given by the sample surface) are still not routinely achieved with nanometer precision, especially at room temperature in water. High-

resolution visual position sensing and reliable alignment of the AFM to arbitrary surface objects are mainly performed under supervision by external microscopy, namely, by optical or scanning electron microscopes (SEM). First, in this manner, fully automated processes were achieved under low temperature high vacuum conditions with special AFM/SEM hybrids, which allow the controlled picking and placement of nano-objects on micro-electromechanical systems (MEMS)¹⁵ to assemble novel nano-devices.

In biophysical applications, however, where aqueous ambients and physiological temperatures are needed, the realization of the AFM as a nano-handling robot working fully automated on artificial structures is still challenging, although various applications of such high control are considered: from the analysis of non-trivial electric or magnetic field properties in structured surroundings to the controlled characterization and individual assembly of single molecules in the coordinate system of present objects. The critical issue in these applications is the highly indispensable positional control of the AFM tip. The mentioned AFM/SEM combination is performing in ultra high vacuum (UHV) and so excludes adequate conditions for most biophysical applications. Localization by conventional optical microscopes may be sufficient for a reliable positioning of the AFM on the microscale. On the nanoscale, however, new superresolution approaches seem required to overcome the diffraction limited resolution. As a third option, many research instruments in this field perform accurate tip-sample alignment by topographic scans

^{a)}Electronic mail: diana.pippig@physik.uni-muenchen.de

coarsely aligned to the region of interest. After imaging, the cantilever tip is positioned on a certain feature in the scanned region.¹⁶ Unfortunately, this method harbors several shortcomings: typical acquisition times of topographic imaging hamper fast tip localizations, as they are required for automated nanohandling. For example, operations on different objects with undefined micrometer to millimeter distances to each other would turn out to be time-consuming and thus impractical if topographic scans for each of the individual objects had to be recorded. Additionally, AFM imaging is not capable of returning steady positional feedback, so an initial alignment is prone to instrumental drift. Without steady optical feedback, errors of the automated progress cannot be actively controlled or corrected. By working to a great extent blindly, a once established tip-object distance has to be maintained with nanometer accuracy by stabilizing the whole system with secondary drift compensations. Additionally, in some biophysical applications, contact-mode scans are unfavorable if a complex surface chemistry on sample and tip is utilized. Prolonged contact between tip apex and sample surface leads to interactions and physical damage, which either rubs off the elaborate functionalization of the tip surface or comes along with clogging of the cantilever.¹⁶ Both effects prevent or at least diminish specific interactions between tip and surface.

To overcome these localization challenges, we developed a fast and non-invasive optical technique of tip localization and subsequent alignment to specific nano-objects with nanometer accuracy. Processing the absorption profile of commercial silicon cantilevers in transmission microscopy by background correction and superresolution based fitting algorithms^{17,18} provides a spatial accuracy below 6 nm.

II. EXPERIMENTAL METHOD

Most advanced AFM instruments are combined with optical microscopes. Already, a simple transmission microscope allows identifying coarse surface structures on the sample and a rough alignment of cantilever and specific surface objects for further scanning procedures. This limited alignment is based on the absorbance of the cantilever resulting in a shadow image in the transmission microscope. We present an advancement of

this localization-by-absorption principle via superresolution routines that allows locating the position of a cantilever's tip to an accuracy, which is substantially better than the diffraction limited microscope resolution. Thus, relative positions of surface objects to the tip are determined to a much higher precision than their actual signal widths.

The general principle is depicted in Figure 1: Whereas light in the visible range propagates through the cantilever to a great extent, the fraction of light incident on the high aspect-ratio tip is strongly absorbed. This is based on the fact that the absorption lengths of typical cantilever materials used in force spectroscopy lie in the same range as their tip lengths. For example, crystalline silicon with an absorbance length of about $1.8 \mu\text{m}$ in the visible spectrum (at 600 nm)¹⁹ is rather transparent for a cantilever thickness typically in the range of a few hundred nanometers, whereas the tip with a length of several micrometers is significantly longer than this typical absorption length. An additional gold layer evaporated on the cantilever for enhanced laser beam reflection is typically below 50 nm and hence transmits about 10% of the illumination in the visible spectrum (for 40 nm gold layer thickness, 9% of the light are transmitted at 600 nm). The observed absorption signal is isolated for further superresolution approaches by background subtraction routines.

Due to the geometry of tip and illumination, the distinct absorption profile is only distinguishable from the background, if the tip apex is in the microscope's focus. For a non-coherent illumination source of a conventional light-emitting diode (LED) used in transmission microscopy, the objective collects light in a limited range of angles in the upper half space (Figure 2(b)). This illumination angles are mainly determined by the extension and distance of the illuminating light source and not by the numerical aperture of the microscope. For a cantilever apex angle comparable to the angles of illumination, the fraction of absorbed light becomes only significant in close vicinity to the imaged plane (Figure 2(b), right). For a distance of about 5 cm between cantilever and LED illumination with an extension of approximately 1 cm, a maximum illumination angle of about 6° is estimated. This opening angle compares to the apex angle of the used tip (BL-AC40TS, Olympus) of about 4° (Figure 2(a)).

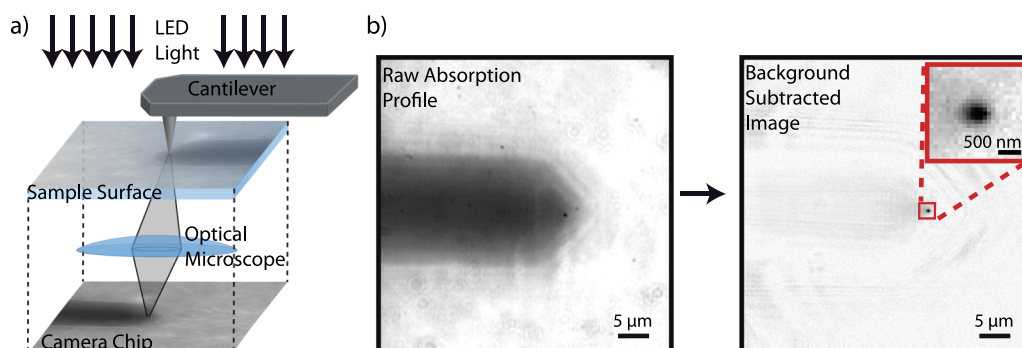


FIG. 1. (a) Schematic representation of the fast and non-invasive localization process of a cantilever tip using transmission microscopy. Incident light is significantly absorbed within the high-aspect ratio tip whereas it transmits the cantilever to a great part. Thus, the tip absorption profile can be clearly identified in the microscope's image plane. (b) Since the background signal, mainly consisting of absorption and scattering of the cantilever, remains nearly constant during tip-surface approach, subtraction of a non-contact image yields a remarkably enhanced signal quality for further localization algorithms.

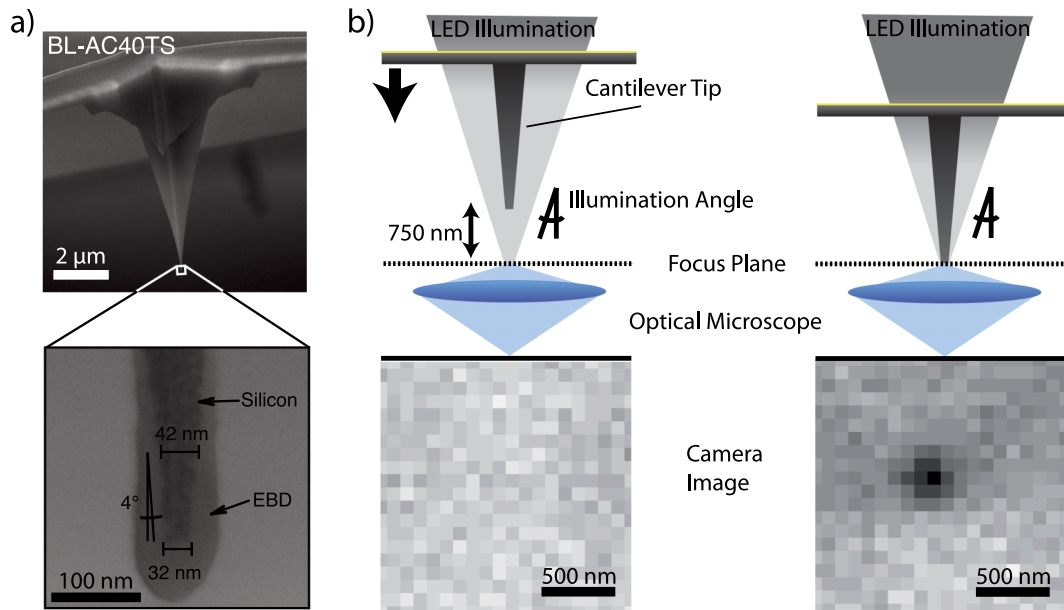


FIG. 2. (a) Width and apex angle of the cantilever tip used for localization imaged in a scanning electron microscope. An apex angle of about 4° is measured. The electron beam deposition (EBD) is no intrinsic property of the cantilever and hence does not contribute to the extension of the imaged tip. (b) The microscope's focus plane images light of an illuminating light source for a given range of incident angles. Extension and distance of the light source determine the maximum illumination angle, for which light can be collected. For comparable angles of the illumination cone and tip apex, the tip is imaged only in close vicinity to the focal plane. For distances larger than 750 nm, however, in the presented experiment, non-absorbed background light surpasses the absorbance signal by the tip.

For increasing distance to the image plane, light passing the cantilever without being absorbed surpasses the absorbance signal of the tip. Depending on the ratio of maximum illumination angle and apex angle of the tip, its absorbance is only detectable when being below a certain distance to the image plane. Since image plane and sample surface are usually aligned for surface-based applications, the absorption signal becomes visible only when the tip is in touch with the surface. However, experimental variation of the distance between sample surface and focal plane yielded that the tip's absorption profile is independent of its vicinity to the glass surface. The observed absorption is not based on near-field effects caused by the proximity to the glass (Figure 3). Further, spectral limitation of the used white-light LED to monochromatic light using different filters in the light path did not change the absorption profile compared to a full-spectrum white-light LED (data not shown).

As a superposition of absorbed and scattered light from both, tip and cantilever, the absorption profile may be far from a perfect two-dimensional point-spread function, but still a projection of a punctuate object below the diffraction limit of the imaging system. The details within the spot will stay unresolved, but the mid-position of the spot, and hence the location of the tip, should be determinable with sub-diffractional precision by reasonable post-processing and superresolution routines.

The absorption profile collected by the microscope can be subdivided into two parts: a weak, static fraction given by the cantilever itself and a strong punctuate spot induced by the tip. For typical approach distances of an AFM to the surface in the micrometer range, the tip is out of focus and—as was shown above—cannot be localized or identified by absorption. During surface approach, the tip acts like a foreground

object—in front of a maintained background—being only visible in close proximity to the surface. As a consequence, an image subtraction of an unfocused referencing frame allows to extract the “purified absorption profile” of the tip. Suppressing the static background during AFM approach drastically improves the signal quality for further localization routines. It should be mentioned here, that for long-term stability of the methodology, a permanent sharp focus on the surface plane is of particular importance. In order to compensate for focus drifts, auto-focus routines are indispensable to maintain optimum localization accuracy.

A more detailed study of the change in absorption signal with respect to AFM distance from the surface gives an optimum distance range for the referencing image dependent on used optics and microscope resolution. It turns out that the selection of the right distance for reference and signal frame is a fundamental factor for reliable localizations. It should be chosen as close as possible to the surface, but without the tip absorption being already distinguishable from the cantilever background signal. Setting the background frame too close to the surface results in loss of useful tip data. Appropriate selection of the referencing height is further discussed in the supplementary material.²⁰

After extracting the absorption profile of the tip, the signal still shows characteristic asymmetries. These may, to a certain extent, originate from optical distortions of the microscope itself as well as aberrations for imaging the extended three-dimensional object. Since the tip is an object with asymmetric geometry, the absorption signal always features certain asymmetries independent of the optics. Figure 4 shows a close-up of the tip absorption signal with and without background subtraction. The signal is spread over only a small number of pixels, each corresponding to a size of about 90 nm. For this image

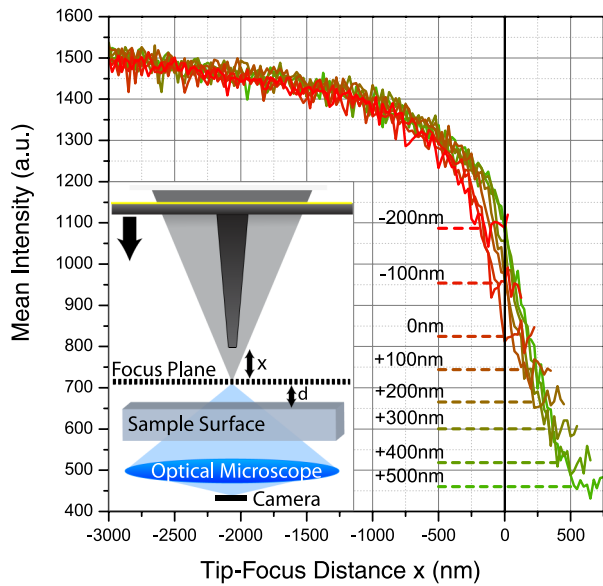


FIG. 3. For a $900 \text{ nm} \times 900 \text{ nm}$ image area around the determined tip position, the intensity during AFM approach is recorded in order to investigate the effect of different distances between surface and the microscope's focal plane (see inset for schematic principle). As a general behavior, it can be seen that the background light exceeds the tip absorption signal for distances larger than 750 nm from the focus, so no remarkable intensity change during approach can be observed in this range. For smaller distances, the absorption of the cantilever tip becomes significant and dampens the collected light intensity by absorption. Changing the relative distance between sample surface and the microscope's focus does not affect the properties of cantilever absorption during approach (color gradient from green to red). The variation of surface height is identified by plateaus in the intensity. Since the tip cannot penetrate the glass surface, its minimal height is limited and stays constant for further approach. No near-field effects at the surface interface seem to alter the behavior of the absorption profile. Thus in experimental applications, an autofocus routine can be used to align surface and image plane in a reliable and reproducible manner.

magnification, the pixel size is about the standard deviation of the localized point spread function, an optimal condition for most superresolution applications. The centroid is determined by optimizing a two-dimensional fit between model and data. The fit optimization is based on the Levenberg-Marquardt algorithm.²¹ Usual fitting routines based on two-dimensional elliptical Gaussian peak functions, however, only poorly approximate the absorption profile. Remarkable deviations in the residual provide a means for analyzing the error of the fitting process and thus of the position measurement. Substantial imbalances in the residual for a symmetric Gaussian function indicate an erroneous shift of the determined position. A uniform and low residual signal is therefore essential in order to localize the object. Consequently, in contrast to most superresolution applications, only an adapted fitting function different from a symmetric Gaussian shape is able to model the centroid of the absorption profile with nanometer precision. For adequate fitting accuracies beyond the microscope's resolution, a two-dimensional peaked function is applied featuring different widths for each quadrant, full rotational capability, and a tilted background plane (see Figure S2 in the supplementary material for further details²⁰). Figure 4 illustrates a comparison of fitting procedures without these additional degrees of freedom and reveals remarkable deviations of fit and signal in the residual. Fitting the tip via the adapted function,

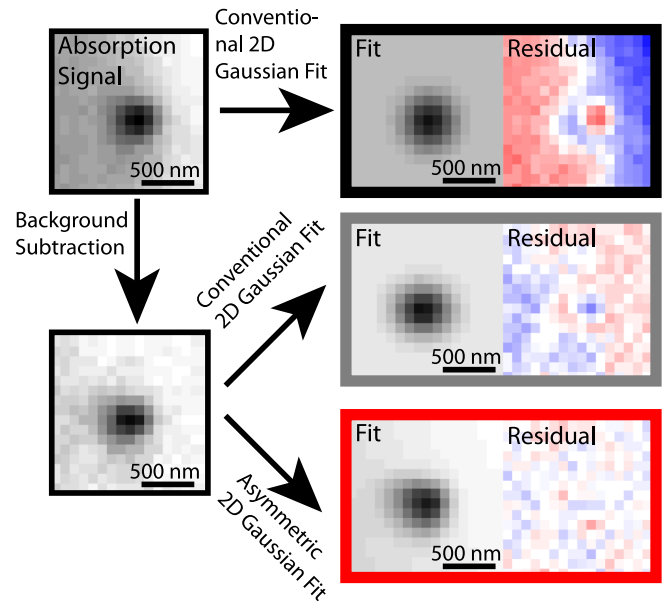


FIG. 4. Fitting an asymmetric signal by a symmetric function yields poor agreement of fit and signal indicated by high imbalances in the residual. Blue color indicates a negative residual whereas red shows a positive contribution to the residual. As a result, the localized position is shifted from the actual mean position (black frame). The applied background correction reduces these asymmetries and improves the object localization via a conventional two-dimensional Gaussian fit, but according to the residual, a positional shift can still be assumed (grey frame). Sophisticated fitting routines based on a non-symmetric Gaussian function featuring four different widths and an implicit rotational angle are able to suppress remaining imbalances in the residual (red frame) and are capable to model the tip absorption adequately.

however, shows fewer imbalances in the residual. The applied model seems to represent the measured absorption profile adequately and hence to determine its mid-position accurately.

III. RESULTS

To evaluate the positional error of the presented localization method, the standard deviation of a statistically significant number of subsequent localizations was investigated. The mid position of each localization process was compared to the overall mean of all determined positions. For signal acquisition, the AFM tip, a BL-AC40TS (Olympus, Japan), was kept in surface contact for longer than the exposure time of the camera. The force threshold for being in surface contact was 180 pN . For about 11.000 absorbed photons, 150 subsequent localizations resulted in a two-dimensional Gaussian uncertainty with a standard deviation of about 5.2 nm (Figure 5(a)). Data points were corrected for directional cantilever drift during the overall measurement time (Figure S3, supplementary material²⁰). The number of photons was determined by counting negative photons with respect to the non-absorbing background average.

After subtracting a referencing background image, the absorption signal can be assumed as shot-noise limited, i.e., the noise in each camera pixel should be dominated by the photons that are transmitted through the localized object and not dominated by background noise. Theoretical limits for shot-noise limited signals scale as the inverse square root of the number of collected photons from the specific object.¹⁷ In Figure

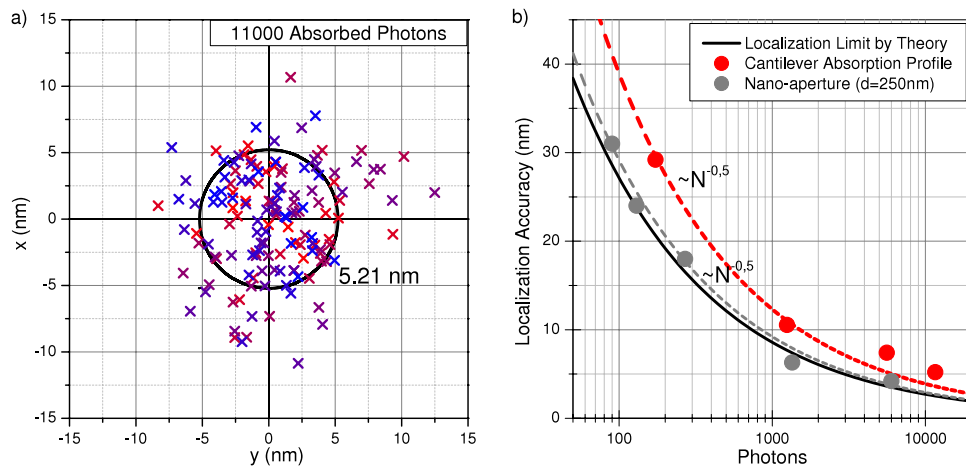


FIG. 5. (a) In superresolution applications, the localization precision of a fluorophore's center via an optical microscope depends fundamentally on the number of collected photons. For a cantilever absorbing about 11 000 photons during exposure time, an accuracy below 6 nm is determined. The accuracy was measured as the two-dimensional standard deviation to the overall mean of a set of several subsequent localizations. The color gradient from red to blue of the data points encodes their temporal evolution with time. A linear thermal drift correction was applied. (b) The theoretical power law for superresolution applications is given by $1/\sqrt{N}$ photons (black curve). A comparison of tip localization based on absorption shows accuracies in the same order of magnitude and equivalent photon dependency as the theoretical limit (red). Determination of the tip's position is apparently feasible with accuracies beyond diffraction. The number of photons represents in this specific case the number of absorbed photons with respect to the measured background signal. For comparison, also the localization precision of a nano-aperture with 220 nm diameter via extraordinary plasmonic transmission is shown (grey). The suitable geometric properties of the aperture—the radial symmetry and a sub-diffraction diameter—yield a transmission signal that can be assumed as a point-spread function without losing localization accuracy.

5(b), the theoretical limit of determining a fluorophore's center is plotted with respect to the number of collected photons (black). The susceptibility of the measurement considering finite microscope resolution (pixelation noise), gain, and camera sensitivity is regarded.

For comparison, the tip localization accuracy via absorption for different numbers of absorbed photons is also depicted. The amount of collected negative photons could be tuned by changing LED power of the transmission microscope as well as the exposure time of the camera. The comparison of the tip localization to the theoretical optimum reveals that, indeed, some accuracy is lost, but it settles in equal orders of magnitude and also obeys the same power law.

For additional comparison, also the localization accuracy of a nano-aperture with 110 nm nominal radius, which acts as a so called zero-mode waveguide,²² is shown in Figure 5(b) for different numbers of collected photons. Zero-mode waveguides are subwavelength holes in the metal coating of glass cover slips, which have no propagating light mode inside their cavity due to their sub-diffractional geometry. Using these structures, the observation volume of optical microscopes can be reduced up to three orders of magnitude compared to diffraction limited optics.^{23,24} The transmitted light used for localization arises from photons tunneling through the nano-cavity via extraordinary plasmonic transmission.^{25,26} The results show that the more adequate geometry of the sub-diffraction nano-aperture can be assumed to be a perfect point-spread function without losing localization precision compared to a fluorophore. Since both, AFM tip and zero-mode waveguide, are objects not affected by photobleaching, more photons per time as well as in absolute number can be obtained compared to fluorophores. Localization of photostable sub-diffractional objects keeps the potential of accuracies even better than those usually obtained in conventional superresolution applications.

The following set of experiments quantitatively investigates the overall accuracy for the presented localization method with subsequent alignment to a specific surface object, e.g., a zero-mode waveguide. As presented before, the individual localization accuracy for a cantilever tip as well as for a zero-mode waveguide is on the order of 5 nm for sufficient numbers of collected (negative) photons. This precision should suffice to align the two objects with adequate accuracy to operate with the AFM tip within the zero-mode waveguide. The accessibility of the upper half-space of the zero-mode waveguide sample allows its employment in combination with the AFM. The experiments were performed on an artificially structured surface fabricated by e-beam photolithography²⁷ containing arrays of nano-apertures of about 220 nm in diameter (see Figure 4(a) and the supplementary material).²⁰ The height of the apertures is 100 nm according to the thickness of the evaporated opaque aluminum film. Additional micrometer sized glass areas without aluminum serve for orientation, coarse alignment of the AFM with the microscope's field of view, and for the presented tip localization routine. A custom-written software (LabView) performs in a fully automated manner the previously described background image correction during AFM approach and determines the tip position by fitting an asymmetric Gaussian function to the measured absorption profile. After additionally localizing a specific zero-mode waveguide by its plasmonic transmission profile, both positions in the optical coordinate system are aligned by piezo-driven movement of the sample. A subsequent surface approach of the AFM should be within the respective zero-mode waveguide. For this application, very small apex angles of the cantilever tip as the one used are of particular importance. Simultaneous measurement of the contact point between surface and AFM tip serves as an experimental validation as for whether the approach was inside the aperture and thus whether the alignment of the two objects was successful.

Due to the topography of the apertures, a 100 nm difference for successful and non-successful approaches can be measured (see Figure 6(b)).

For 14 different zero-mode waveguides within one 220 nm size array, the localization and alignment cycle was repeated 50 times each to prove its reliability and reproducibility. Additionally, some approaches next to zero-mode waveguides on aluminum were performed to illustrate the signal for a failed alignment procedure. Zero-mode waveguide and aluminum approaches form two distinct height populations separated by about 100 nm (Figure 6(b), red and blue markers). Of altogether 700 approaches in zero-mode waveguides, only two appear to be not within the aperture by being outliers in the height signal. One cycle was typically performed within 15 s. The sample was sufficiently equilibrated during the preparation of the experiment, so that vertical surface drifts became negligible for the actual measurement. A sample tilt correction was applied to the data by a linear fit. The shown experiment further confirms that the presented localization method allows for a fast, non-invasive, reliable, and reproducible alignment of the AFM with a nano-object like a 220 nm zero-mode waveguide.

In order to give a quantitative number of the alignment precision, the behavior close to a zero-mode waveguide sidewall was additionally investigated. Adding varying spatial offsets to the localized aperture position allows imaging the topography of the aperture. For small offsets, the AFM still operates within the zero-mode waveguide whereas for offsets larger than the diameter, this does not hold any more. Figure 6(c) illustrates the contact height with respect to the offset in a certain direction. For each surface approach, tip localization and aperture alignment were repeated. Two plateaus are

clearly distinguishable for the regions within and outside the aperture linked by a crossing section representing the rim of the zero-mode waveguide. Assuming a perfectly steep topography of the apertures, one would expect a stepwise behavior for this particular region. There are two main reasons for experimentally measured deviations: an extended geometry of the probing tip as well as inaccuracies in the alignment routine. Thus, the standard deviation of the rim region can be taken as an upper limit for the process accuracy neglecting other effects. Excluding points being part of the two identified plateaus (Figure 6(c), red points), a standard deviation of 13 nm for imaging the zero-mode waveguide border is obtained. As an upper limit, this proves the nanoscale precision of the localization and subsequent alignment of the two objects.

To prove that the presented alignment procedure is not only fast and accurate but also does not damage the specific surface chemistry on the cantilever, the applicability of the localization routine in force spectroscopic measurements was tested. The mechanical unfolding of a green fluorescent protein (GFP), covalently immobilized to the bottom of zero-mode waveguides, was addressed. Its typical unfolding pattern could be detected and the characteristic contour length of 77 nm was measured (Figure 7)²⁸ without observing additional features in force-distance curves that would arise from harsh contact of the cantilever with the sidewalls of the aperture. For each force curve, the contact point of tip and surface was noted to ensure that the tip was actually probing within the zero-mode waveguide. Furthermore, in order to prevent unspecific binding of the protein to the surface, the aluminum was passivated for protein binding sites by polyvinylphosphonic acid.²⁹ In a total of 850 recorded force curves distributed over 11 different zero-mode waveguides, 40 specific binding

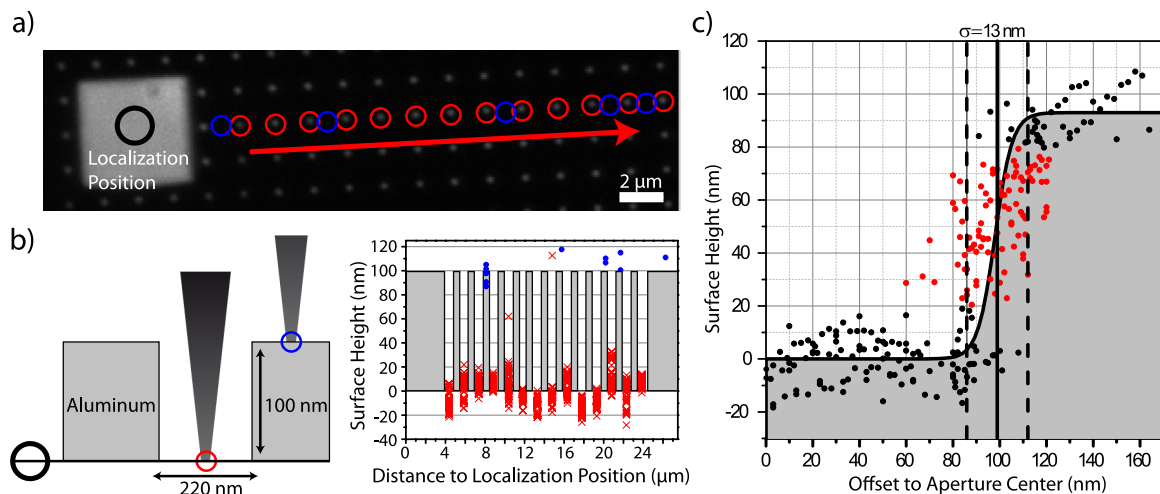


FIG. 6. (a) The presented localization allows a fast and reliable alignment of cantilever and a given sample structure, e.g., an array of nano-apertures in transmission microscopy. To demonstrate the high reliability of the method, the tip was localized repeatedly in a specifically designed localization area and subsequently aligned with a zero-mode waveguide array (220 nm diameter and 100 nm height). (b) For each zero-mode waveguide, the localization process was repeated 50 times. As control parameter for successful alignment, the height at which surface and tip get in first contact is used as illustrated by the schematic principle. Blue markers represent tip approaches next to cavities on aluminum to illustrate the signal for non-successful alignment processes. For 700 fully automated approaches within 14 zero-mode waveguides (red), only two cycles can be clearly identified as non-successful, i.e., not inside the specific zero-mode waveguide. (c) Quantitative accuracy of the complete alignment process is checked by tip approaches with controlled offset within one zero-mode waveguide. After center alignment of zero-mode waveguide and cantilever, a specific offset in a certain spatial direction is added. By repeating the process for different offsets, the sidewall of the cavity gets imaged with a measurable uncertainty. The steep rim is mapped with an accuracy of 13 nm, giving a quantitative number for the alignment precision. Since contributions by the extended geometry of the cantilever tip and a non-ideal edge steepness of the zero-mode waveguide are neglected, the measured value can be assumed as an upper accuracy limit.

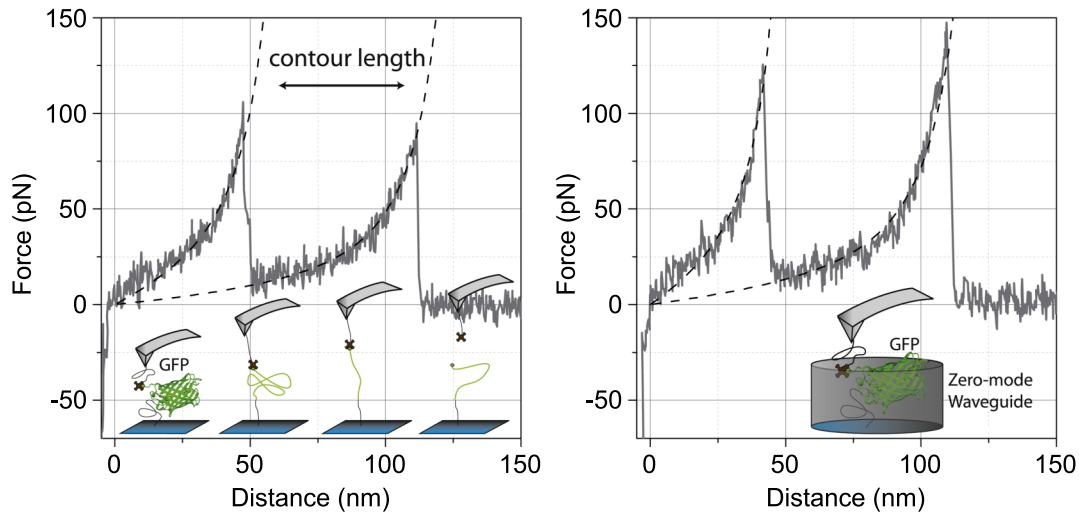


FIG. 7. One possible application of the presented alignment procedure is high-throughput force spectroscopy inside the nano-apertures of zero-mode waveguides. Single GFP unfolding events with characteristic contour lengths are depicted. Comparison to rupture events on a glass reference of the same sample confirms that the characteristic unfolding behavior is not altered when measured inside a zero-mode waveguide.

events could be observed in less than 2 h. This represents a successful binding efficiency of almost 5%, which is in total agreement to the efficiency of a subsequent control experiment on a pure glass area on the same sample with the same lateral density of immobilized proteins on the surface. In future applications, a conventional fluorescence microscope, such as a total internal reflection fluorescence (TIRF) microscope, should be simultaneously triggered and force-distance information should be simultaneously collected by the AFM. Such custom-built hybrid setups combining atomic force with TIRF microscopy were developed in previous work and will allow for high-throughput force spectroscopy in zero-mode waveguides with simultaneous fluorescence read-out.³⁰

Strong anticipated applications of the presented tip localization method with subsequent nano-structure alignment are single-molecule cut and paste arrangements of enzymatic circuits like replication machineries or cellulosomes and furthermore force spectroscopy in zero-mode waveguides.^{31,16} With high throughput efficiencies comparable to those of standard force spectroscopy, the presented approach could become state-of-the-art in the biomolecular research of force-activated biomolecules³² by direct observation of enzymatic substrate turnover.³³ Since zero-mode waveguides are applicable to most biophysical assays,^{23,34–36} this optomechanical methodology could give insight into many mechanoenzymatic processes obscured so far, especially on the single-molecule level. In contrast to other localization routines, the presented superresolution methodology using the tip's absorption profile offers the necessary requisites for high-throughput experiments with efficiencies comparable to those in common force spectroscopy.

IV. CONCLUSION

Being able to localize an AFM tip with nanoscale precision in the coordinate system of a sample with macroscopic dimensions grants access to a wide range of novel applications,

be it in nanoprecision manufacturing or sophisticated single molecule research. Here, we demonstrated that conventional optical transmission microscopy in combination with elaborate image analysis allows to localize the AFM tip with more than 6 nm precision with reference to the optical axis of the microscope. The large actuation ranges of the microscope stage now allow addressing large sample areas with this novel technique. At the same time, a precision is achieved that allows to investigate individual molecules. Remarkably, the elaborate functionalization of the probe, which is indispensable to such sensitive measurements, is unimpaired by the localization process. This could be verified by the single-molecule force spectroscopy unfolding experiment on individual GFPs in the apertures of a zero-mode waveguide.

ACKNOWLEDGMENTS

The authors would gratefully thank Professor Philip Tinnefeld for helpful discussions, Philipp Altpeter and Ellis Durner for technical support, and Magnus Bauer for experimental assistance. This work was supported by the Advanced ERC Grant Cellufuel, the SFB1032, the VolkswagenStiftung, and the Nanosystems Initiative Munich (NIM).

- ¹G. Binnig, C. F. Quate, and C. Gerber, *Phys. Rev. Lett.* **56**(9), 930 (1986).
- ²M. Radmacher, M. Fritz, H. G. Hansma, and P. K. Hansma, *Science* **265**(5178), 1577 (1994).
- ³S. M. Lindsay, L. A. Nagahara, T. Thundat, U. Knipping, R. L. Rill, B. Drake, C. B. Prater, A. L. Weisenhorn, S. A. Gould, and P. K. Hansma, *J. Biomol. Struct. Dyn.* **7**(2), 279 (1989).
- ⁴M. Radmacher, R. W. Tillmann, M. Fritz, and H. E. Gaub, *Science* **257**(5078), 1900 (1992).
- ⁵E. L. Florin, V. T. Moy, and H. E. Gaub, *Science* **264**(5157), 415 (1994).
- ⁶M. Rief, M. Gautel, F. Oesterhelt, J. M. Fernandez, and H. E. Gaub, *Science* **276**(5315), 1109 (1997).
- ⁷F. Oesterhelt, D. Oesterhelt, M. Pfeiffer, A. Engel, H. E. Gaub, and D. J. Müller, *Science* **288**(5463), 143 (2000).
- ⁸S. K. Kufer, E. M. Puchner, H. Gump, T. Liedl, and H. E. Gaub, *Science* **319**(5863), 594 (2008).
- ⁹D. M. Eigler and E. K. Schweizer, *Nature* **344**(6266), 524 (1990).
- ¹⁰M. T. Cuberes, R. R. Schlittler, and J. K. Gimzewski, *Appl. Phys. Lett.* **69**(20), 3016 (1996).

- ¹¹T. Junno, K. Deppert, L. Montelius, and L. Samuelson, *Appl. Phys. Lett.* **66**(26), 3627 (1995).
- ¹²C. Baur, A. Bugacov, B. E. Koel, A. Madhukar, N. Montoya, T. R. Ramachandran, A. A. G. Requicha, R. Resch, and P. Will, *Nanotechnology* **9**(4), 360 (1998).
- ¹³R. M. Sullan, A. B. Churnside, D. M. Nguyen, M. S. Bull, and T. T. Perkins, *Methods* **60**(2), 131 (2013).
- ¹⁴G. M. King, A. R. Carter, A. B. Churnside, L. S. Eberle, and T. T. Perkins, *Nano Lett.* **9**(4), 1451 (2009).
- ¹⁵M. F. Yu, M. J. Dyer, G. D. Skidmore, H. W. Rohrs, X. K. Lu, K. D. Ausman, J. R. Von Ehr, and R. S. Ruoff, *Nanotechnology* **10**(3), 244 (1999).
- ¹⁶S. F. Heucke, F. Baumann, G. P. Acuna, P. M. Severin, S. W. Stahl, M. Strackharn, I. H. Stein, P. Altpeter, P. Tinnefeld, and H. E. Gaub, *Nano Lett.* **14**(2), 391 (2014).
- ¹⁷R. E. Thompson, D. R. Larson, and W. W. Webb, *Biophys. J.* **82**(5), 2775 (2002).
- ¹⁸A. Yildiz and P. R. Selvin, *Acc. Chem. Res.* **38**(7), 574 (2005).
- ¹⁹M. A. Green and M. J. Keevers, *Prog Photovoltaics* **3**(3), 189 (1995).
- ²⁰See supplementary material at <http://dx.doi.org/10.1063/1.4915145> for further details on applied background correction, fitting function, drift corrections, microscope setups as well as sample preparation and fabrication.
- ²¹J. J. Moré, *Lect. Notes Math.* **630**, 105 (1977).
- ²²P. Zhu and H. G. Craighead, *Annu. Rev. Biophys.* **41**, 269 (2012).
- ²³K. T. Samiec, M. Foquet, L. Guo, E. C. Cox, and H. G. Craighead, *Biophys. J.* **88**(3), 2145 (2005).
- ²⁴M. J. Levene, J. Korlach, S. W. Turner, M. Foquet, H. G. Craighead, and W. W. Webb, *Science* **299**(5607), 682 (2003).
- ²⁵T. W. Ebbesen, H. J. Lezec, H. F. Ghaemi, T. Thio, and P. A. Wolff, *Nature* **391**(6668), 667 (1998).
- ²⁶C. Sonnichsen, A. C. Duch, G. Steininger, M. Koch, G. von Plessen, and J. Feldmann, *Appl. Phys. Lett.* **76**(2), 140 (2000).
- ²⁷M. Foquet, K. T. Samiec, X. X. Kong, B. P. Chaudhuri, P. M. Lundquist, S. W. Turner, J. Freudenthal, and D. B. Roitman, *J. Appl. Phys.* **103**(3), 034301 (2008).
- ²⁸H. Dietz and M. Rief, *Proc. Natl. Acad. Sci. U. S. A.* **101**(46), 16192 (2004).
- ²⁹J. Korlach, P. J. Marks, R. L. Cicero, J. J. Gray, D. L. Murphy, D. B. Roitman, T. T. Pham, G. A. Otto, M. Foquet, and S. W. Turner, *Proc. Natl. Acad. Sci. U. S. A.* **105**(4), 1176 (2008).
- ³⁰H. Gumpf, S. W. Stahl, M. Strackharn, E. M. Puchner, and H. E. Gaub, *Rev. Sci. Instrum.* **80**(6), 063704 (2009).
- ³¹S. F. Heucke, E. M. Puchner, S. W. Stahl, A. W. Holleitner, H. E. Gaub, and P. Tinnefeld, *Int. J. Nanotechnol.* **10**(5-7), 607 (2013).
- ³²E. M. Puchner and H. E. Gaub, *Annu. Rev. Biophys.* **41**, 497 (2012).
- ³³E. M. Puchner, A. Alexandrovich, A. L. Kho, U. Hensen, L. V. Schafer, B. Brandmeier, F. Grater, H. Grubmüller, H. E. Gaub, and M. Gautel, *Proc. Natl. Acad. Sci. U. S. A.* **105**(52), 21045 (2008).
- ³⁴T. Miyake, T. Tani, H. Sonobe, R. Akahori, N. Shimamoto, T. Ueno, T. Funatsu, and I. Ohdomari, *Anal. Chem.* **80**(15), 6018 (2008).
- ³⁵J. M. Moran-Mirabal, A. J. Torres, K. T. Samiec, B. A. Baird, and H. G. Craighead, *Nanotechnology* **18**(19), 195101 (2007).
- ³⁶J. Eid, A. Fehr, J. Gray, K. Luong, J. Lyle, G. Otto, P. Peluso, D. Rank, P. Baybayan, B. Bettman, A. Bibillo, K. Bjornson, B. Chaudhuri, F. Christians, R. Cicero, S. Clark, R. Dalal, A. Dewinter, J. Dixon, M. Foquet, A. Gaertner, P. Hardenbol, C. Heiner, K. Hester, D. Holden, G. Kearns, X. Kong, R. Kuse, Y. Lacroix, S. Lin, P. Lundquist, C. Ma, P. Marks, M. Maxham, D. Murphy, I. Park, T. Pham, M. Phillips, J. Roy, R. Sebra, G. Shen, J. Sorenson, A. Tomaney, K. Travers, M. Trulson, J. Vieceli, J. Wegener, D. Wu, A. Yang, D. Zaccarin, P. Zhao, F. Zhong, J. Korlach, and S. Turner, *Science* **323**(5910), 133 (2009).

Supporting Information:

Tip localization of an atomic force microscope in transmission microscopy with nanoscale precision

Fabian Baumann¹, Stephan F. Heucke², Diana A. Pippig^{1,a)}, and Hermann E. Gaub¹

¹ Center for Nanoscience and Department of Physics, University of Munich, Amalienstraße 54, 80799 Munich, Germany

² Center for Integrated Protein Science Munich (CIPSM), University of Munich, Amalienstraße 54, 80799 Munich, Germany

I. SUPPLEMENT

A. Choosing the background distance

Subtracting the adequate reference image isolates efficiently the tip signal for further routines by reducing the constant cantilever background. For this process, however, the choice of the right referencing frame is fundamental to guarantee a reliable localization with high accuracy. In order to investigate the localized position dependent on which images are taken for it, a wide comparison for different combinations of background and signal frames was performed. The complete AFM approach is recorded as a full set of image frames. By knowing the approach velocity as well as the contact point of AFM and surface, each frame can be associated with a tip-surface-distance. In the case presented here, the AFM approaches linearly with about 12.5 nm per each image frame. For the whole image set, any possible combination of signal frame m and background image n was taken for localizing the tip coordinates $x_{m,n}$ and $y_{m,n}$. It turns out, that for tip distances larger than 200 nm the tip signal is too blurry for stable convergence of the Gaussian fit. For background frames closer than 300 nm, important signal information is apparently subtracted leading to a non-convergent fit as well (figure S1a). For image combinations within these respective distance limits, meaningful localization positions are obtained. In order to further evaluate the reliability of different image combinations the stability of their specific localization is checked. To do so, the spatial standard deviation $s_{m,n}(x_{m,n}, y_{m,n})$ for signal image m and a set of neighboring background images $[n-2; n+2]$ was calculated. For a stable and hence reliable combination of two images, it was assumed, that small variations of the background image should not result in high fluctuations of the localized position. Figure S1a illustrates that a stable region (i.e. smallest $s_{m,n}$ values) is found for the tip being in surface contact combined with a background image in about 600 to 800 nm distance.

This result is in good agreement of findings investigating at which distances the tip absorption signal becomes distinguishable from the cantilever background. For a camera image of $1 \mu\text{m} \times 1 \mu\text{m}$ at contact position, the mean image intensity is plotted during surface approach. For a starting distance of 2000 nm, the mean intensity within the area does not change significantly at first. The tip absorbance is out of focus and therefore not imaged by the microscope whereas the cantilever background stays rather constant. For distances smaller than 750 nm, however, the image mean becomes drastically reduced by the strong absorbance of the tip (figure S1b). Since the tip absorbance is not predominant until 750 nm sur-

face distance, the referencing frame can be chosen here without losing important tip signal by subtraction, but still providing a background profile as close as possible. In the fully automated software routine, a region of interest at the tip's position is chosen and the mean intensity during approach is recorded. Out of these values the change from stagnant to declining behavior is measured in order to define an adequate picture as a reference frame. The actual signal profile is always best during surface contact. All of the measurements as well as the presented data here were done after an autofocus routine in order to have reliable results.

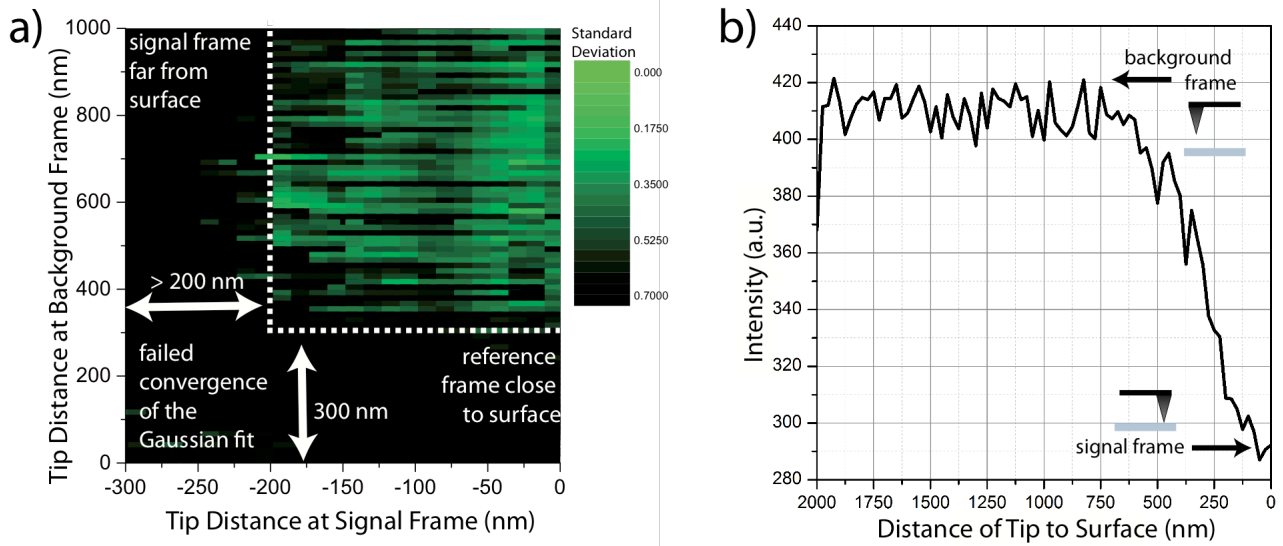


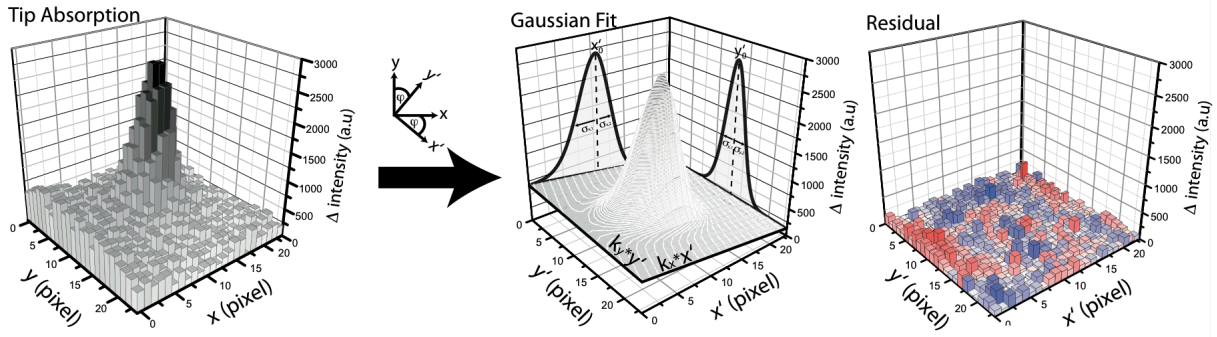
FIG. S1.

- a) Standard deviation of the determined tip position for different combinations of signal and background distances. Stable convergence of the Gaussian fit is only given for the tip in close proximity of the surface and a minimal distance between signal and background frame of at least 300 nm. The standard deviation has a stable minimum plateau for tip and background frames at a distance between 600 and 800 nm to each other indicating best signal qualities there.
- b) Mean intensity of $1 \mu\text{m} \times 1 \mu\text{m}$ region of interest during tip approach. The absorption of the tip becomes only measurable for distances less than 750 nm to the surface. Choosing a background frame with a tip distance larger than 750 nm no important signal information is lost during background subtraction

B. Asymmetric Gaussian fit

The adapted asymmetric Gaussian fitting function features the following parameters:

- A : amplitude of the peaked function
- φ : rotational angle of the 2D coordinate system $(x, y) \Rightarrow (x', y')$
- x_0', y_0' : peak position
- $\sigma_{x,1}, \sigma_{x,2}, \sigma_{y,1}, \sigma_{y,2}$: for each half-plane in x' or y' the Gaussian width changes at mid-point x_0', y_0'
- k_x, k_y : modeling a tilted background plane
- C : constant background level



$$G(x,y) = Ae^{-\frac{(x'-x'_0)^2}{2\sigma_{x,i}^2} - \frac{(y'-y'_0)^2}{2\sigma_{y,j}^2}} + k_x x' + k_y y' + C$$

$$\begin{cases} i = 1 & \forall x' > x'_0 \\ i = 2 & \forall x' \leq x'_0 \\ j = 1 & \forall y' > y'_0 \\ j = 2 & \forall y' \leq y'_0 \end{cases}$$

with $x' = x \cos(\varphi) + y \sin(\varphi)$ and $y' = y \cos(\varphi) - x \sin(\varphi)$

FIG. S2.

Example for modeling the absorption of a cantilever tip by an adapted Gaussian fit. The signal features an asymmetric shape for both coordinate axes as well as a tilted background plane. The coordinate axes are capable to rotate in the horizontal plane for adapting the asymmetries of the tip signal. For improved illustration, but without loss of generality, the shown example yields $\varphi=0^\circ$ for horizontal rotation. The color-code in the residual illustrates regions of negative (blue) or positive (red) difference between fit and signal. Only small imbalances are observed indicating a reliable modeling of the absorption signal.

C. Linear drift correction of localized tip

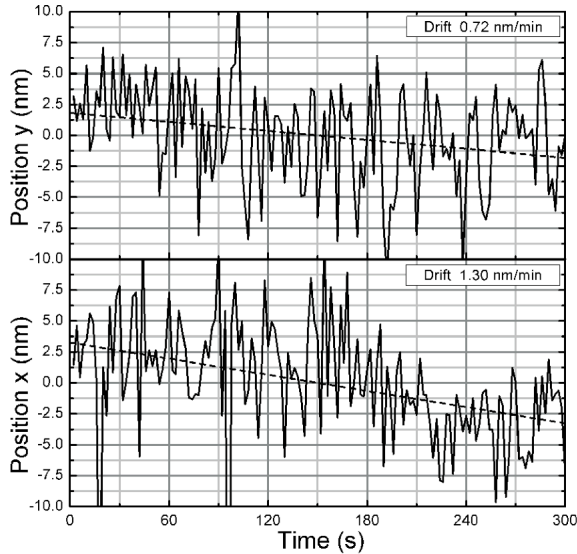


FIG. S3.

Correction method for systematic positional drift of the cantilever tip during measurement of the experimental localization accuracy. A linear fit is applied to the data and subtracted. In this data set (11000 photons per localization), a drift of about one nanometer per minute is detected. The sample was settled on the experimental setup for several hours before measurement to minimize drift effects during data collection.

D. AFM measurements

A custom built AFM head and an Asylum Research MFP3D controller (Asylum Research, Santa Barbara, USA), which provides ACD and DAC channels as well as a DSP board for setting up feedback loops, were used. Software for the automated control of the AFM head and xy-piezos during the experiments was programmed in LabView and Igor Pro (Wave Metrics, Lake Oswego, USA). Cantilevers were calibrated in solution using the equipartition theorem^{1,2}.

E. Zero-mode waveguide lithography

Zero-mode waveguide samples were fabricated with negative e-beam lithography similar to [3] and [4]. The diameters of the zero-mode waveguides used in the localization experiments were measured afterwards with scanning electron microscopy (figure S4).

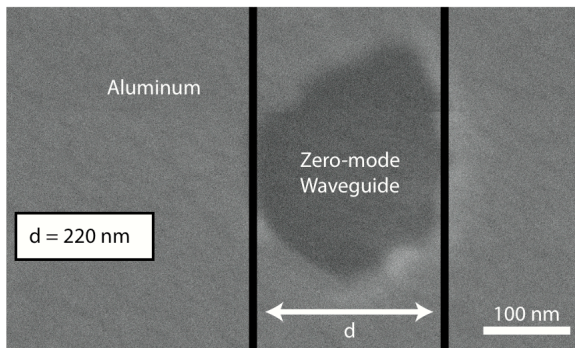


FIG. S4. Scanning electron microscopy image of a representative zero-mode waveguide used in the shown alignment with the cantilever tip.

F. Preparation of the sample surface

After cleaning of the samples as described in [4] and chemically selective passivation of the aluminum on the surface⁵ the samples were incubated in 3-aminopropyltrimethoxysilane (ABCRC, Karlsruhe) for 5 minutes. Subsequently, they were washed in toluol, 2-propanol and ddH₂O and dried at 80 °C for 30 min. After deprotonation in sodium borate buffer (50mM H₃BO₃, 50mM Na₂B₄O₇•10 H₂O pH=8.5; Carl Roth GmbH & Co. KG, Germany) for 1 hour, a heterobifunctional PEG crosslinker with N-hydroxy succinimide and maleimide groups (MW 5000, Rapp Polymere, Tübingen, Germany) was applied for 30 minutes at 12.5 mM in sodium borate buffer. The slide was thoroughly washed with ddH₂O, before it was incubated another hour with Coenzyme A (Merck Millipore, USA) dissolved in coupling buffer (50mM NaHPO₄, 50mM NaCl, 10mM EDTA at pH=7.2). Again the slide was washed with ddH₂O.

A superfolder GFP⁶ construct was used and attached to the surface via an N-terminal ybbR-tag (DSLEFIASKLA)⁷. Expression and protein purification were according to [8]. Via a Phosphopantetheinyltransferase Sfp-mediated coupling strategy⁹ the Coenzyme A on the glass slide was linked to the ybbR-tag of the protein in humid atmosphere at room temperature during three hours incubation time. For this, the protein construct GFP was mixed with Sfp-buffer (120 mM TrisHCl pH7.5, 10 mM MgCl₂, 150 mM NaCl, 2% Glycerol, 2 mM DTT) and Sfp-Synthetase. All protein that did not bind to the surface was washed off step-wise by 15ml 1xPBS. This buffer was also used for the force spectroscopy measurements.

II. REFERENCES

- ¹E. L. Florin, M. Rief, H. Lehmann, M. Ludwig, C. Dornmair, V. T. Moy, and H. E. Gaub, *Biosens Bioelectron* 10 (9-10), 895 (1995).
- ²H. J. Butt and M. Jaschke, *Nanotechnology* 6 (1), 1 (1995).
- ³M. Foquet, K. T. Samiec, X. X. Kong, B. P. Chauduri, P. M. Lundquist, S. W. Turner, J. Freudenthal, and D. B. Roitman, *J Appl Phys* 103 (3) (2008).
- ⁴S. F. Heucke, F. Baumann, G. P. Acuna, P. M. Severin, S. W. Stahl, M. Strackharn, I. H. Stein, P. Altpeter, P. Tinnefeld, and H. E. Gaub, *Nano letters* 14 (2), 391 (2014).
- ⁵J. Korlach, P. J. Marks, R. L. Cicero, J. J. Gray, D. L. Murphy, D. B. Roitman, T. T. Pham, G. A. Otto, M. Foquet, and S. W. Turner, *Proceedings of the National Academy of Sciences of the United States of America* 105 (4), 1176 (2008).
- ⁶J. D. Pedelacq, S. Cabantous, T. Tran, T. C. Terwilliger, and G. S. Waldo, *Nat Biotechnol* 24 (9), 1170 (2006). 7J. Yin, A. J. Lin, D. E. Golan, and C. T. Walsh, *Nat Protoc* 1 (1), 280 (2006).
- ⁷J. Yin, A. J. Lin, D. E. Golan, and C. T. Walsh, *Nat Protoc* 1 (1), 280 (2006).
- ⁸D. A. Pippig, F. Baumann, M. Strackharn, D. Aschenbrenner, and H. E. Gaub, *Acs Nano* 8 (7), 6551 (2014).
- ⁹J. Yin, P. D. Straight, S. M. McLoughlin, Z. Zhou, A. J. Lin, D. E. Golan, N. L. Kelleher, R. Kolter, and C. T. Walsh, *Proceedings of the National Academy of Sciences of the United States of America* 102 (44), 15815 (2005).
- ¹⁰J. L. Zimmermann, T. Nicolaus, G. Neuert, and K. Blank, *Nat Protoc* 5 (6), 975 (2010). [
- ¹¹S. Voss and A. Skerra, *Protein Eng* 10 (8), 975 (1997).